Mitochondrial activity and biogenesis during resurrection of Haberlea rhodopensis

Aneta Ivanova, Santiago Signorelli, Denis Falconet, Daniela Moyankova, James Whelan, Dimitar Djilianov, Monika Murcha

New Phytologist

Research

Mitochondrial activity and biogenesis during resurrection of *Haberlea rhodopensis*

Aneta Ivanova[1,2], Brendan O'Leary[1,3], Santiago Signorelli[1,4], Denis Falconet[5], Daniela Moyankova[2], James Whelan[6], Dimitar Djilianov[2] and Monika W. Murcha[1]

[1]School of Molecular Sciences, The University of Western Australia, 35 Stirling Highway, Crawley, Perth, WA 6009, Australia; [2]AgroBioInstitute, Agricultural Academy, 8 Dragan Tzankov Blvd., 1164, Sofia Bulgaria; [3]Saskatoon Research and Development Centre, Agriculture and Agri-Food Canada, 107 Science Place, Saskatoon, SK K1A 0C5, Canada; [4]Department of Plant Biology, School of Agriculture, Universidad de la República, E. Garzón 780, Sayago, 12900 Montevideo, Uruguay; [5]Cell and Plant Physiology Laboratory, CNRS, CEA, INRAE, IRIG, Université Grenoble Alpes, 38054 Grenoble, France; [6]Department of Animal, Plant and Soil Science, School of Life Science, The ARC Centre of Excellence in Plant Energy Biology, La Trobe University, Bundoora, 3086, VIC, Australia

Authors for correspondence
Monika W. Murcha
Email: monika.murcha@uwa.edu.au

Dimitar Djilianov
Email: d_djilianov@abi.bg

Received: *4 April 2022*
Accepted: *11 July 2022*

New Phytologist (2022) **236:** 943–957
doi: 10.1111/nph.18396

Key words: desiccation tolerance, *Haberlea rhodopensis*, mitochondria, mitochondrial biogenesis, respiration, resurrection plants.

Summary

- *Haberlea rhodopensis* is a resurrection plant that can tolerate extreme and prolonged periods of desiccation with a rapid restoration of physiological function upon rehydration. Specialized mechanisms are required to minimize cellular damage during desiccation and to maintain integrity for rapid recovery following rehydration.
- In this study we used respiratory activity measurements, electron microscopy, transcript, protein and blue native-PAGE analysis to investigate mitochondrial activity and biogenesis in fresh, desiccated and rehydrated detached *H. rhodopensis* leaves.
- We demonstrate that unlike photosynthesis, mitochondrial respiration was almost immediately activated to levels of fresh tissue upon rehydration. The abundance of transcripts and proteins involved in mitochondrial respiration and biogenesis were at comparable levels in fresh, desiccated and rehydrated tissues. Blue native-PAGE analysis revealed fully assembled and equally abundant OXPHOS complexes in mitochondria isolated from fresh, desiccated and rehydrated detached leaves. We observed a high abundance of alternative respiratory components which correlates with the observed high uncoupled respiration capacity in desiccated tissue.
- Our study reveals that during desiccation of vascular *H. rhodopensis* tissue, mitochondrial composition is conserved and maintained at a functional state allowing for an almost immediate activation to full capacity upon rehydration. Mitochondria-specific mechanisms were activated during desiccation which probably play a role in maintaining tolerance.

Introduction

Droughts have devastating impacts on crop production and food security. In this respect, developing crops with increased drought tolerance is a major focus for plant breeders and researchers. Whilst most plants can withstand mild drought for short periods of time, loss of water content below 40% results in extensive damage and ultimately death (Höfler & Rottenburg, 1941). A small group of plants (< 0.2% of the total flora) termed 'resurrection plants' are unique in that they can survive long periods of time desiccated with water content < 10% and recover within hours upon hydration (Oliver *et al.*, 2005, 2020). Whilst desiccation tolerance is observed in ferns, mosses, pollen and orthodox seeds, desiccation tolerance within angiosperm vegetative tissues is a rare phenomenon (Gaff & Oliver, 2013). Consequently, resurrection plants are valuable models to study the molecular mechanisms involved in desiccation tolerance and a comprehensive knowledge of the fundamental mechanisms involved is crucial. The Balkan endemic *Haberlea rhodopensis* can survive unusually long periods of desiccation for ≤ 2 yr and resume normal growth within hours of hydration (Gechev *et al.*, 2013).

Several studies have investigated the physiological, cellular and molecular mechanisms involved in establishing desiccation tolerance. Specialized mechanisms minimize damage and maintain cellular integrity during desiccation and rapidly mobilize cellular function and repair mechanisms upon rehydration (Oliver *et al.*, 2020). Among the core protective mechanisms are the accumulation of late embryogenesis abundant (LEA) proteins, small heat shock proteins (sHSPs) and early light-induced protein (ELIP) (reviewed by Gechev *et al.*, 2021), and osmolytes such as proline (Forlani *et al.*, 2019), proposed to protect proteins from dehydration and aggregation. Sucrose and oligosaccharides accumulate and act as osmoprotectants to stabilize membranes (Martinelli, 2008; Djilianov *et al.*, 2011; Moyankova *et al.*, 2014).

Nonenzymatic and enzymatic antioxidant systems also are activated to establish desiccation tolerance. Located within the energy-producing organelles, mitochondria and chloroplasts, antioxidant molecules such as glutathione, ascorbate, tocopherols and polyphenols have been observed to increase during desiccation (Djilianov *et al.*, 2011; Moyankova *et al.*, 2014; Georgieva *et al.*, 2017). Scavengers such as superoxide dismutase, ascorbate peroxidase, catalase and glutathione reductase also accumulate during desiccation (Gechev *et al.*, 2013), probably to prevent reactive oxygen species (ROS) damage.

The specific role of chloroplasts (and photosynthesis) has been determined during the desiccation of several resurrecting species (Koonjul *et al.*, 2000; Dinakar *et al.*, 2012; Mladenov *et al.*, 2015; Georgieva *et al.*, 2020; Nadal *et al.*, 2021). Inhibition of photosynthesis is a central response, observed in both desiccation-tolerant and desiccation-sensitive plants affected by drought (Challabathula *et al.*, 2018). Desiccation of sensitive plants leads to irreparable damage of the photosynthetic membranes, however, in desiccation-tolerant resurrecting plants, the photosynthetic apparatus is deactivated during desiccation, followed by complete recovery upon rehydration. Two mechanisms have been described for this process; (i) poikilochlorophyllous plants degrade chlorophyll (Chl) and the photosynthetic apparatus in a regulated manner requiring *de novo* synthesis during rehydration (Tuba *et al.*, 1998) whilst (ii) homoiochlorophyllous plants preserve Chl and thylakoid membranes and instead initiate active protection mechanisms. The homoiochlorophyllous *H. rhodopesis* maintains chloroplast morphology, preserving the integrity of the thylakoid membrane, photosystems I (PSI) and II (PSII) and a high Chl content during desiccation, and initiate protective mechanisms during desiccation to prevent damage and maintain the integrity of the photosynthetic apparatus (Georgieva *et al.*, 2020). Molecular responses protecting photosynthetic machinery include the upregulation of genes encoding early light-inducible proteins (ELIP), LEA, antioxidant enzymes and cell-wall modification enzymes (Gechev *et al.*, 2013; Liu *et al.*, 2018).

Plant mitochondria play an essential role in energy production, are a major nexus of carbon and nitrogen metabolism, and play critical roles linked to photosynthesis and in responses to oxidative and environmental stresses. Unlike photosynthesis, mitochondrial function during desiccation has not been well-studied in resurrection plants. Tuba *et al.* (1997) reported that mitochondrial respiration rates correlated to tissue water content in *Xerophyta humilis* (Tuba *et al.*, 1997). Likewise, respiration rates declined only after drying to 40% relative water content (RWC) in the homoiochlorophyllous species *Craterostigma wilmsii* and *Myrothamnus flabellifolius*, whilst in the poikilochlorophyllous monocot *Xerophyta humilis*, respiration rates declined when RWC decreased to 20% and ceased in all three species at ≤ 10% (Farrant, 2000). Recently, a comprehensive transcriptomic, proteomic and metabolic study on *Craterostigma plantagineum* has provided some insight into the role of mitochondria in desiccation tolerance (Xu *et al.*, 2021). RNA-Seq analysis data showed a high abundance of transcripts encoding mitochondrial protein import components *TIM17* and *TIM23*, suggesting an upregulation of mitochondrial biogenesis during desiccation, in addition to an accumulation of tricarboxylic acid cycle (TCA) intermediates and oxidative phosphorylation (OXPHOS) machinery (Xu *et al.*, 2021). These findings suggest mitochondrial biogenesis and activity may be maintained during desiccation, to minimize ROS damage and provide an energy advantage upon rehydration.

Here we investigated mitochondrial activity during the dehydration and subsequent rehydration of detached *H. rhodopensis* leaves with an emphasis on the role of mitochondria in desiccation tolerance. We found that mitochondrial respiration is established almost immediately upon rehydration and before the reactivation of photosynthesis. Transcript and protein abundance of proteins involved in mitochondrial biogenesis are high in desiccated leaves and remain constant during rehydration, along with fully assembled oxidative phosphorylation machinery. Furthermore, the alternative respiratory components and mitochondrial stress-responsive components were observed to be most abundant in desiccated tissues suggesting that specific mitochondrial mechanisms play a role in maintaining organelle integrity during desiccation and allow for rapid activation of function.

Materials and Methods

Plant material and growth conditions

Haberlea rhodopensis Friv. plants were propagated *in vitro* (Djilianov *et al.*, 2005) and then transferred to soil. The plants were grown for 1 yr at a temperature of 24°C, 16 h : 8 h, light : dark photoperiod of 40 μmol m^{-2} s^{-1} and 40–60% relative humidity. For desiccation, fully developed young leaves were detached, weighed (100%: initial FW, IFW) and air-dried for 3, 6, 12, 24, 36, 48, 60 and 72 h until 15% of the IFW was achieved. Rehydration was carried out on a wet filter paper for 3, 6, 12, 24, 36, 48, 60 and 72 h at room temperature. Weight during desiccation and recovery was determined as a percentage of the leaf weight relative to the IFW.

Oxygen consumption measurements

Oxygen (O_2) consumption measurements on leaf tissue were conducted in the dark and at 21°C at 1-min intervals using a Q2 oxygen sensor (Astec-Global) with minor modifications (O'Leary *et al.*, 2017). Leaf tissue (*c.* 20 mg desiccated or 50 mg fresh or rehydrated) was placed in a sealed 5-ml capacity tubes and partially submerged in 400 μl of water. The slope of O_2 consumption was calculated according to Scafaro *et al.* (2017) between 0.5 and 20 h after the start of the run. The experiment was repeated three times with ≥ 12 replicates for each treatment. Samples also were analyzed with the addition of HCN, 40 μl of 0.1 M KCN added to 150 μl of 1 M KOH in a 200-μl tube, that was placed inside the sealed 5-ml tube to generate gaseous HCN.

Chlorophyll fluorescence-related parameters

Chlorophyll fluorescence was measured using the MAXI-Imaging PAM fluorometer system (Heinz Walz, Effeltrich, Germany; Barbagallo *et al.*, 2003). Leaves were treated and dark-adapted for 20 min and their fluorescence was determined during 800 ms exposure to a saturating pulse, having a photon flux density (PFD) of 4800 μmol m^{-2} s^{-1}. From the variable and maximal

fluorescence, the maximum quantum efficiency of PSII was calculated as F_V/F_M in three different areas of interest (AOI) of each leaf (technical replicates) and at least three leaves (biological replicates) for each treatment were used for the analysis. An ANOVA analysis was performed including an honestly significant difference (HSD) Tukey–Kramer's *post hoc* test and those with *P*-values < 0.05 were consider statistically significantly different. Immediately after F_V/F_M determination, from the same AOI, leaves, and number of replicates, the chloroplast electron transport rate (ETR) parameter was determined. Twenty measurements were used to describe the light curve for ETR, from 0 to 1076 photosynthetic active radiation (PAR, μmol quanta m^{-2} s^{-1}), with a 20-s gap between measurements. The ETR of technical replicates were combined to get the leaf ETR, and the ETR of different leaves for the same treatment were plotted to get the treatment ETR trend. A loess regression was adjusted to each curve with a 95% confidence interval using the R package GGPLOT2.

Pearson correlation analysis

Pearson correlation analysis were performed between F_V/F_M and percentage of rehydration to determine if there is a positive and significant correlation. Therefore, the average of F_V/F_M and percentage of rehydration for each treatment were plotted as scatter plot in *R* and a Pearson correlation test was performed to determine the Pearson correlation coefficient, *P*-value and its biological significance. This was done using the whole dataset and by separating the data into two sets, as two phases seem to be present based on the scatter plot profile.

Transmission electron microscopy

Leaves were processed according to Flori *et al.* (2018). Samples were infiltrated with ethanol/Epon resin mixture and embedded in Epon. Ultrathin sections (50–70 nm) were prepared with a diamond knife on a PowerTome ultramicrotome and collected on 200-μm nickel grids. Ultrathin sections were examined on a Philips CM120 transmission electron microscope operating at 80 kV.

Mitochondrial isolation

Mitochondria were isolated from fresh, desiccated and 72-h rehydrated *H. rhodopensis* leaves using a modified method initially described for rice embryos (Howell *et al.*, 2006). Briefly, about 0.4 g desiccated and 2 g of fresh or rehydrated leaf tissue were homogenized using pre-chilled mortar and pestle in 100-ml mitochondrial grinding media (0.3 M sucrose, 50 mM tetrasodium pyrophosphate, 2 mM EDTA, 0.5% (w/v) PVP-40, 0.5% BSA, 20 mM cysteine, pH = 7.5). The cell debris and chloroplasts were pelleted by centrifugation at 2500 ***g*** for 5 min. The supernatant, containing mitochondria, was centrifuged at 17 500 ***g*** for 20 min, the pellet was resuspended in wash buffer (0.3 M sucrose, 10 mM TES, pH 7.5), and layered over a Percoll™ step gradient consisting of 3 ml 40% Percoll™, 3 ml 25% Percoll™, 3 ml 15% Percoll™ in wash buffer, centrifuged at 34 000 ***g*** for 30 min, 4°C without brakes. The mitochondrial band visible at the 25–40% Percoll™ interface was removed, and washed in 50-ml wash buffer, and centrifuged at 22 000 ***g*** for 15 min at 4°C.

Respiratory complex activity measurements

All enzymatic assays were carried out using isolated mitochondria and performed at 25°C using a spectrophotometer (UV-1800; Shimadzu, Kyoto, Japan) over a period of 2 min in triplicate. Complex I, II, IV, Pyruvate decarboxylase (PDC) and malate dehydrogenase (MD) assays were carried out as described in Huang *et al.* (2015). Ubiquinol-cytochrome c reductase (Complex III) activity was measured by the reduction of cytochrome c (Luo *et al.*, 2008). ATP synthase (Complex V) activity was measured according to Catterall & Pedersen (1971).

Oxygen consumption measurements in isolated mitochondria

Oxygen consumption from isolated mitochondria (100 μg protein) was measured using Oxytherm Clark-type Electrodes (Hansatech, King's Lynn, UK) in 1 ml of air-saturated respiration media (300 mM sucrose, 10 mM NaCl, 5 mM KH_2PO_4, 2 mM $MgSO_4$, 0.1% (w/v) BSA, 10 mM TES. pH 7.2) at 25°C (Jacoby *et al.*, 2015). The respiratory chain first was activated with 200 nM ADP whichever substrate was being used and the rate of O_2 uptake was calculated between 1.5 and 3.5 min after adding ADP. Oxygen consumption assay for total mitochondrial electron transport chain (ETC)-linked respiration was performed in the presence of 1 mM nicotinamide adenine dinucleotide, reduced (NADH) and 5 mM succinate. The capacity for electron flux through the alternative oxidase (AOX) pathway was obtained as the rate of O_2 consumption in the presence of 1 mM cyanide (KCN). The AOX pathway was activated by a mix of 1 mM pyruvate and 5 mM dithiotreitol (DTT) and then inhibited with 0.1 mM *n*-propyl gallate (nPG). Uncoupled respiration capacity was measured in the presence of 1 mM NADH and 5 mM succinate and after permeabilization of the inner mitochondrial membrane to protons, which dissipates the proton gradient by addition of the 5 μM ionophore FCCP (carbonyl cyanide-*p*-trifluoromethoxyphenylhydrazone). Total TCA-linked respiration was evaluated in the presence of mixture of cofactors (2 mM nicotinamide adenine dinucleotide, oxidized (NAD^+), 200 μM Coenzyme A (CoA) and 12 μM thiamine pyrophosphate (TPP)) and respiratory substrates (10 mM malate and 10 mM pyruvate).

Immunoblotting

Mitochondrial and total proteins, extracted according to Wang *et al.* (2006) were separated using SDS-PAGE, transferred to PVDF and immunodetected using antibodies raised against *Arabidopsis thaliana* (Arabidopsis) proteins; anti-NADH Dehydrogenase 6 (NAD6; Lamattina *et al.*, 1993), anti-75 kDa of the respiratory chain Complex I (PhytoAb, San Jose, CA, USA), anti-Carbonic anhydrase-like 1 (CAL1) (PhytoAb), anti-Rieske iron sulfur protein (RISP) (Carrie *et al.*, 2010), anti-Cytochrome c oxidase 2 (COX2) (Agrisera, Vasterbotten, Sweden), anti-

NADH:ubiquinone oxidoreductase iron sulfur protein 4 (NDUFS4) and anti-Succinate Dehydrogenase subunit 1 (SDH1-1; Zhu *et al.*, 2020), anti-beta subunit ATP synthase (β-ATP) (Agrisera) anti-Alternative NAD(P)H Dehydrogenase 1 (NDA1; Carrie *et al.*, 2009), anti-NAD(P)H Dehydrogenase B2 (NDB2; Soole & Smith, 2015), anti-Alternative Oxidase 1a (AOX1a; Elthon *et al.*, 1989), anti-METAXIN (Lister *et al.*, 2007), anti-Translocase Outer Membrane subunit 40 (TOM40; Carrie *et al.*, 2008), anti-Translocase Inner Membrane subunit 50 (TIM50; Y. Wang *et al.*, 2012), anti-Uncoupling protein (UCP; Considine *et al.*, 2001), anti-Serine hydroxymethyltransferase (SHMT; Agrisera). For each immunoblot, band intensity was measured using ImageJ software. A value of 1 was assigned to band pixel density in fresh tissue and samples normalized relative to it. Three independent biological replicates were carried out.

Blue native PAGE analysis

Blue native (BN)-PAGE analysis was carried out as described previously (Eubel *et al.*, 2005) using 5% (w/v) digitonin and precast 4–16% Bis-Tris gels (Novex™ Life Technologies, Carlsbad, CA, USA). Blue native-PAGE gels were transferred to PVDF and immunodetected.

RNA isolation and transcript analysis

Total RNA was isolated using an RNA isolation Kit (Favorgen Biotech Corp./Fisher Biotec, Subiaco, WA, Australia) according to the manufacturer's instructions. Three independent RNA preparations were performed for each dehydration/rehydration stage (technical triplicates) and assayed in biological replicate. Two micrograms of RNA were converted to cDNA using the HighCapacity cDNA synthesis kit (Bio-Rad) according to the manufacturer's instructions. A value of 1.0 was assigned to the sample with the highest cDNA concentration and the concentrations of other samples were calculated relative to it to calculate a coefficient for normalizing the transcript abundance measured in a quantitative reverse transcription PCR (qRT-PCR) reaction. qRT-PCR was carried out using the LightCycler 480 instrument (Roche) with SYBR Green I master kit (Roche). Primers for all transcripts were designed according to sequences published previously (Gechev *et al.*, 2013; Liu *et al.*, 2018) listed in Supporting Information Table S1.

Statistical analysis

Statistical analysis was done using single-factor ANOVA ($\alpha = 0.05$), followed by Tukey–Kramer's *post hoc* test ANOVA analysis to test the statistically different datasets.

Results

Desiccated *Haberlea rhodopensis* leaves exhibit high respiration rates upon hydration

Haberlea rhodopensis can survive long periods of desiccation and resume normal growth within hours of re-watering. To investigate cellular activity during the desiccation and subsequent rehydration of detached *H. rhodopensis* leaves, a dehydration and rehydration series was carried out over a 72 h period (Fig. 1a). Fresh leaves lost 85% of their IFW within a period of 60 h retaining the remaining 15%, with leaves shrivelling and curling throughout the time course (Figs 1a i, S1a i). Upon hydration, the dry and shrivelled leaves were observed to expand in size and weight, and exhibited reduced leaf curling with the weight recovery increasing from 15% to *c.* 90% relative to the IFW, over 72 h hydration (Figs 1a ii, S1a ii). To determine if mitochondrial activity was restored upon rehydration, O_2 consumption rates were measured using a fluorophore-based oxygen sensor at minute intervals with tissues partially submerged in water. The O_2 consumption rates were measured over a 20-h time period and compared to that of fresh detached *H. rhodopensis* leaves (Fig. 1b i). Averaged O_2 consumption rates were observed to be steady ranging from 0.04 to 0.07 $\mu mol\ s^{-1}\ g\ FW^{-1}$ over the time-course for both desiccated and fresh leaf samples (Fig. 1b i). In addition, O_2 consumption rates of 72-h rehydrated leaves also were measured and compared to fresh detached leaves over a 20-h time period (Fig. 1b ii) and found to be comparable to fresh tissue, indicating that mitochondrial respiration was rapidly activated in desiccated tissue and rates were comparable to that of fresh and 72-h rehydrated leaves.

Haberlea rhodopensis is known to contain several metabolites that accumulate during desiccation which could potentially react with oxygen and affect the O_2 consumption rates. To test for this, KCN, an inhibitor of OXPHOS Complex IV was added to the reaction tube. The presence of KCN reduced O_2 consumption by *c.* 90% ± 1 (Fig. S1b i–ii) indicating that any O_2 consumption rates measured were largely due to mitochondrial respiration. To determine the O_2 consumption rates of nonhydrated desiccated tissue, dark O_2 consumption rates also were measured as above, but in vials without the presence of water, and no O_2 consumption was identified (Fig. S1b iii).

Photosynthetic performance is restored upon rehydration

In order to investigate if photosynthetic performance was recovered during the rehydration time-course and whether it correlated with the percentage of weight recovery, we tested the maximum quantum yield of PSII (F_V/F_M) in fresh, desiccated and rehydrated for 3-, 6-, 12-, 24-, 36-, 48-, 60- and 72-h leaves. We observed that F_V/F_M was reduced to zero in desiccated tissue but increased substantially by 3 h post-rehydration (corresponding to 20% of the IFW), followed by a steady increase until 24 h post-rehydration (80% IFW) when values reached those obtained in fresh leaves (Figs 1c i, S2a). The F_V/F_M positively correlated with the percentage of recovery and water uptake, respectively, in a biphasic manner – at earlier stages of rehydration the F_V/F_M increased faster, whereas, after 60% of recovery, corresponding to 24 h post-hydration, the changes in F_V/F_M were less noticeable (Fig. 1c ii). Chloroplast ETR were reduced dramatically in desiccated leaves and a continued improvement was observed from 6 h post-rehydration (30% IFW) to 48 h post-rehydration (75% IFW) where the ETR was equivalent to that observed in fresh

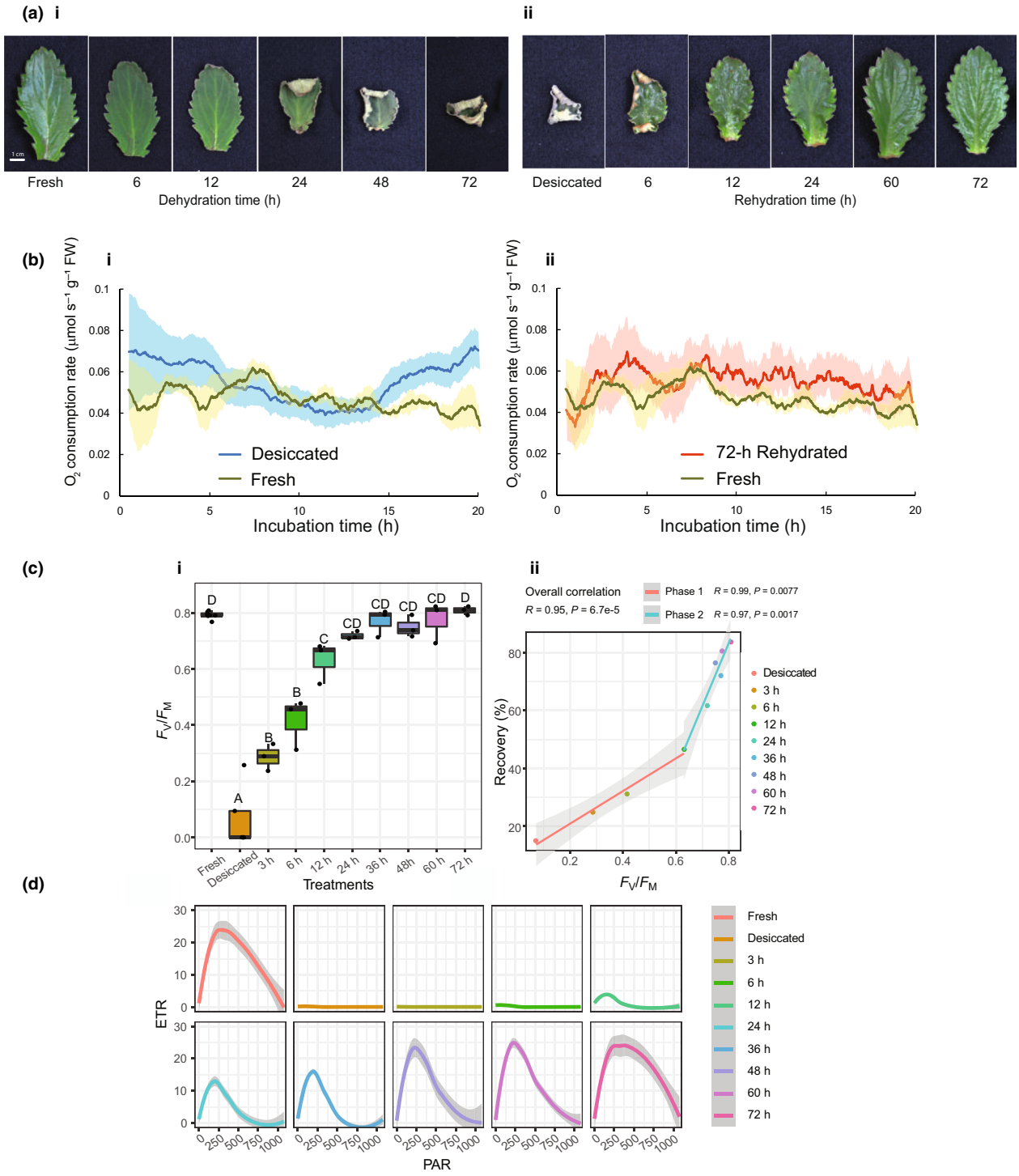

Fig. 1 Dehydration and rehydration of detached *Haberlea rhodopensis* leaves. (a) Stages of desiccation and rehydration, fresh leaf air-dried for 6–72 h (i) and rehydrated from 0 fully desiccated to 72 h post-hydration (ii). (b) Oxygen consumption rates per gram of tissue ($n = 12$) from desiccated and fresh tissues (i) and from 72-h rehydrated and fresh tissues (ii). (c) Photosynthetic performance of fresh, desiccated and rehydrated leaves. (i) Maximum quantum yield of photosystem II (F_V/F_M) in fresh, desiccated and rehydrated leaves. Each dot represents the F_V/F_M of an independent biological replicate (including outliers), whiskers represent the minimum and maximum values, the horizontal line represents the median and the lower and upper boxes represent the 25th and 75th percentiles, respectively. Different letters indicate statistically significant differences in a honestly significant difference Tukey–Kramer's *post hoc* test, $P < 0.05$, $n \geq 3$. (ii) Pearson correlation analysis between F_V/F_M and recovery (%). The overall correlation includes all of the points in the graph (Supporting Information Fig. S2a). Instead, two phases were represented as a linear regression. In all the cases the correlation test is significant. The grey area indicates a 95% confidence interval (CI) for the linear regression. (d) Chloroplast electron transport rates (ETR) for fresh, desiccated and rehydrated leaves. The grey area indicates a 95% CI for the regression applied (LOESS). No overlap between grey areas indicates statistically significant differences (Fig. S2b).

leaves (Figs 1d, S1a, S2b). Maximum ETR was reached following 48 h of rehydration, reaching levels of fresh tissue at 72 h suggesting that the photoprotective mechanisms were not fully recovered until 72 h and thus they cannot cope with high light intensity resulting in a premature decrease (PAR equivalent to 250 μmol quanta m^{-2} s^{-1}) in ETR compared to fresh leaves (Figs 1d, S2b).

Mitochondrial and chloroplast morphology in desiccated leaf tissue

Morphological examination of *H. rhodopensis* mesophyll mitochondria and chloroplasts from fresh, desiccated and 72-h rehydrated tissue was performed using TEM. Both organelles appear to retain integrity during desiccation (Fig. 2a,b). In desiccated leaves, mitochondria appeared smaller but with high electron density and defined cristae structures like that observed in fresh tissue (Fig. 2a,b). In desiccated tissue, the chloroplasts appeared less electron-dense with fewer thylakoid structures and stacked grana compared to those observed in fresh tissue (Fig. 2b). Both organelles appeared completely recovered after 72 h of hydration (Fig. 2c).

Mitochondrial components are preserved in an active state during desiccation

In order to further investigate mitochondrial activity in fresh, desiccated and rehydrated *H. rhodopensis* tissue and compare it with the activity in fresh tissue, mitochondria were isolated using a modified Percoll™ density gradient method. This method involved immediate cellular homogenization of tissue upon coming in contact with grinding buffer, allowing for the isolation of sufficient mitochondria for biochemical and physiological analyses. SDS-PAGE analysis and Coomassie staining of isolated mitochondria from fresh, desiccated and rehydrated tissue displayed comparable protein banding patterns (Fig. S3a). To confirm that the isolated fraction contained enriched mitochondrial proteins, an immunoblot was carried out using an antibody raised against the mitochondrial Translocase of the Inner Membrane 50 (TIM50). Immunodetection was carried out using total protein extract and mitochondrial fraction indicating that the mitochondrial isolation fraction was enriched for mitochondrial proteins (Fig. S3b).

Oxidative phosphorylation consists of four complexes on the inner membrane (complexes I, II, III, IV) whereby electron flow coupled to proton translocation drives ATP synthesis via ATP synthase. To investigate OXPHOS integrity, assembly, abundance and activity, we carried out a series of experiments, including BN-PAGE, enzyme activity assays and O_2 consumption measurements in isolated mitochondria from fresh, desiccated and 72-h rehydrated tissue. To determine the assembly and abundance of OXPHOS complexes, mitochondria were resolved on BN-PAGE and immunodetected with various antibodies against complexes I, II, III, IV and ATP synthase (Fig. 3). The well-characterized OXPHOS complexes from Arabidopsis were resolved alongside (Senkler *et al.*, 2017; Fig. 3a). Immunodetection with antibodies specific for individual subunits of complexes I–V confirms comparable complex abundance and resolution in mitochondria isolated from fresh, desiccated and rehydrated tissues (Fig. 3b–f). Complex I resolved at *c.* 1000 kDa, Complex II at *c.* 200 kDa (with an additional band observed at *c.* 400 kDa), Complex III at *c.* 500 kDa, and Complex IV at *c.* 300 kDa from fresh, desiccated and rehydrated mitochondria (Fig. 3b–e). Antibodies raised against the β-subunit of ATP synthase detected a band of *c.* 600 kDa (Fig. 3f). Therefore, it could be concluded that all OXPHOS complexes were present at similar abundances in mitochondria isolated from fresh, desiccated and rehydrated tissue. Furthermore, the OXPHOS complexes resolved at similar sizes from mitochondria isolated from fresh, desiccated and post-hydrated tissue suggesting that they were fully assembled.

Enzyme activity assays for individual OXPHOS complexes I, II, III, IV and ATP synthase exhibited no substantial differences

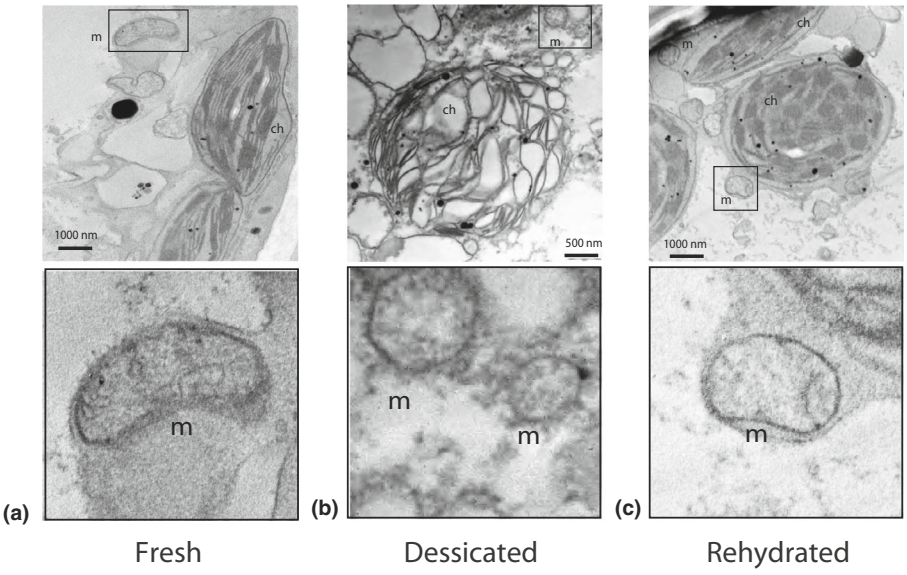

Fig. 2 Organelle ultrastructure in fresh, desiccated and rehydrated *Haberlea rhodopensis* transmission electron micrographs of detached fresh (a), desiccated (b) and 72-h rehydrated (c) leaf tissue. M, mitochondria; Chl, chloroplasts. Bar, 500 or 1000 nm.

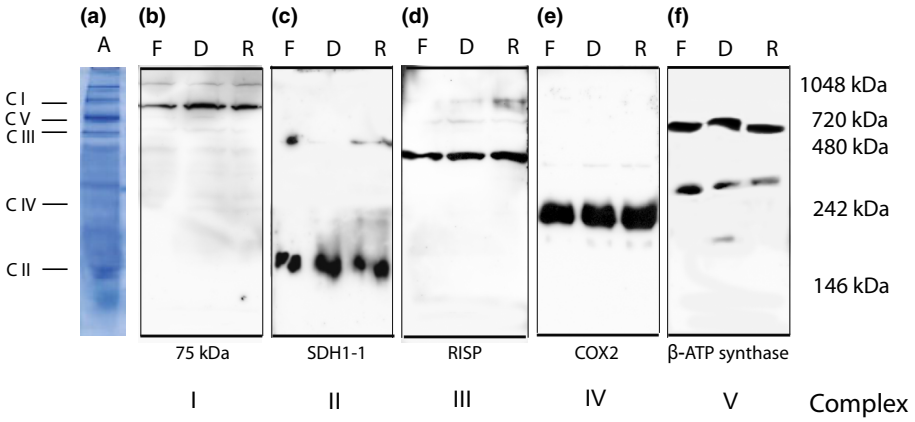

Fig. 3 Mitochondrial oxidative phosphorylation (OXPHOS) complexes are fully assembled and abundant in desiccated and rehydrated *Haberlea rhodopensis* mitochondria. Blue native (BN)-PAGE analysis and immunodetection of *H. rhodopensis* mitochondrial OXPHOS complexes isolated from fresh (f) desiccated (d) and 72-h rehydrated (R) leaf tissue. (a) BN-PAGE analysis and Coomassie staining of Arabidopsis (a) mitochondria indicating the positions of OXPHOS complexes. (b–f) Immunodetection of *H. rhodopensis* mitochondria with (b) anti-75 kDa Complex I subunit, (c) anti-Succinate Dehydrogenase subunit 1 (SDH1) Complex II subunit, (d) anti-Rieske iron sulfur protein (RISP) Complex III subunit, (e) anti-Cytochrome c oxidase (COX2) Complex IV subunit and (f) anti-beta subunit ATP synthase (β-ATP). Bars indicate the positions of Arabidopsis OXPHOS complexes.

in mitochondria isolated from fresh, desiccated and rehydrated tissues (Fig. 4a i–v). Activity measurements for the TCA cycle enzymes malate dehydrogenase (MDH) and pyruvate dehydrogenase (PDH) likewise exhibited no difference in mitochondria isolated from fresh, desiccated and rehydrated tissues (Fig. 4a vi,vii).

In addition to individual mitochondrial respiratory complexes, we assessed the biological properties of isolated mitochondria from desiccated tissue in comparison with fresh and 72-h rehydrated one by measuring O_2 consumption with Clark-type electrode (Figs 4b, S4). The substrate combination of NADH and succinate delivers reductant directly to the ETC at Complex II and external NAD(P) dehydrogenases and bypasses soluble enzymes of the TCA cycle, assessing the maximal activity of the ETC and respiration rate after adding ADP (Fig. S4a,b). ETC-linked respiration rates in fresh tissue were comparable to those of rehydrated tissue, whereas the rates of O_2 consumption of mitochondria, isolated from desiccated leaves was two-fold lower (Figs 4b, S4a,b). The potential contribution of AOX pathway was determined by activating it with DTT in the presence of pyruvate after inhibiting the ETC with KCN. The capacity for electron flux through the cyanide insensitive pathways was 2.5-fold higher in desiccated tissue compared to fresh ones (Figs 4b, S4a); however, these activities could not be attributed exclusively to AOX because they were not fully inhibited by nPG, an AOX inhibitor, indicating the presence of additional uncoupling components (Fig. S4a ii). The AOX capacity after 72 h of hydration was still higher by 1.5-fold compared to mitochondria, isolated from fresh leaves, suggesting that it takes longer than 72 h to completely restore the pre-desiccation levels (Figs 4b, S4a iii). In addition to the AOX pathway, we measured the total uncoupled O_2 consumption capacity (that includes AOX) by addition of the ionophore FCCP, which permeabilizes the inner membranes to protons, dissipating the proton gradient. After FCCP addition, O_2 consumption is no longer coupled to ATP synthesis. Mitochondria isolated from desiccated and rehydrated tissue exhibit about 25% increase in uncoupled capacity compared to mitochondria from fresh leaves (Figs 4, S4b). TCA cycle activity in the presence of substrates malate and pyruvate and NAD^+ in isolated mitochondria from fresh, desiccated and rehydrated tissue was comparable (Figs 4b, S4c).

Transcript and protein analysis indicates high levels of factors involved in mitochondrial biogenesis in desiccated tissue

In order to further investigate mitochondrial activity and biogenesis in fresh, desiccated and rehydrated tissue, the transcript abundance of individual components involved in mitochondrial activity, biogenesis and redox regulation was investigated (Fig. 5). qRT-PCR analysis of the genes encoding the Complex I subunit 75 kDa displayed relatively constant levels of transcript during desiccation and rehydration (Fig. 5a). Likewise, the additional Complex I component, *NDUFS4*, the mitochondria-encoded *NAD6*, and the plant-specific carbonic anhydrase-like (CAL) domain subunit 1, *CAL1*, showed equal transcript abundance at all time points (Fig. 5a). Analysis of SDH subunits showed core subunits *SDH1* and *SDH5* remained stable during desiccation and rehydration (Fig. 5b). Interestingly the SDH subunit *SDH2.1* decreased during dehydration, followed by an increase during hydration, reaching pre-desiccation levels at 72 h. In contrast to its homolog, *SDH2.3* showed a sharp increase during dehydration, peaking in fully desiccated leaves, exceeding the transcript abundance of the fresh leaves > 160-fold, 6 h post-rehydration *SDH2.3* transcript levels dropped substantially, followed by a steady decline (Fig. 5c). Transcripts for subunits of Complex III (*RISP*), Complex IV cytochrome c oxidase (*COX2*) and ATP synthase (*β-ATP synthase*) showed steady expression levels during dehydration/rehydration (Fig. 5d). Analysis of various mitochondrial protein import components showed stable expression of the inner membrane translocases *TIM23, TIM50*

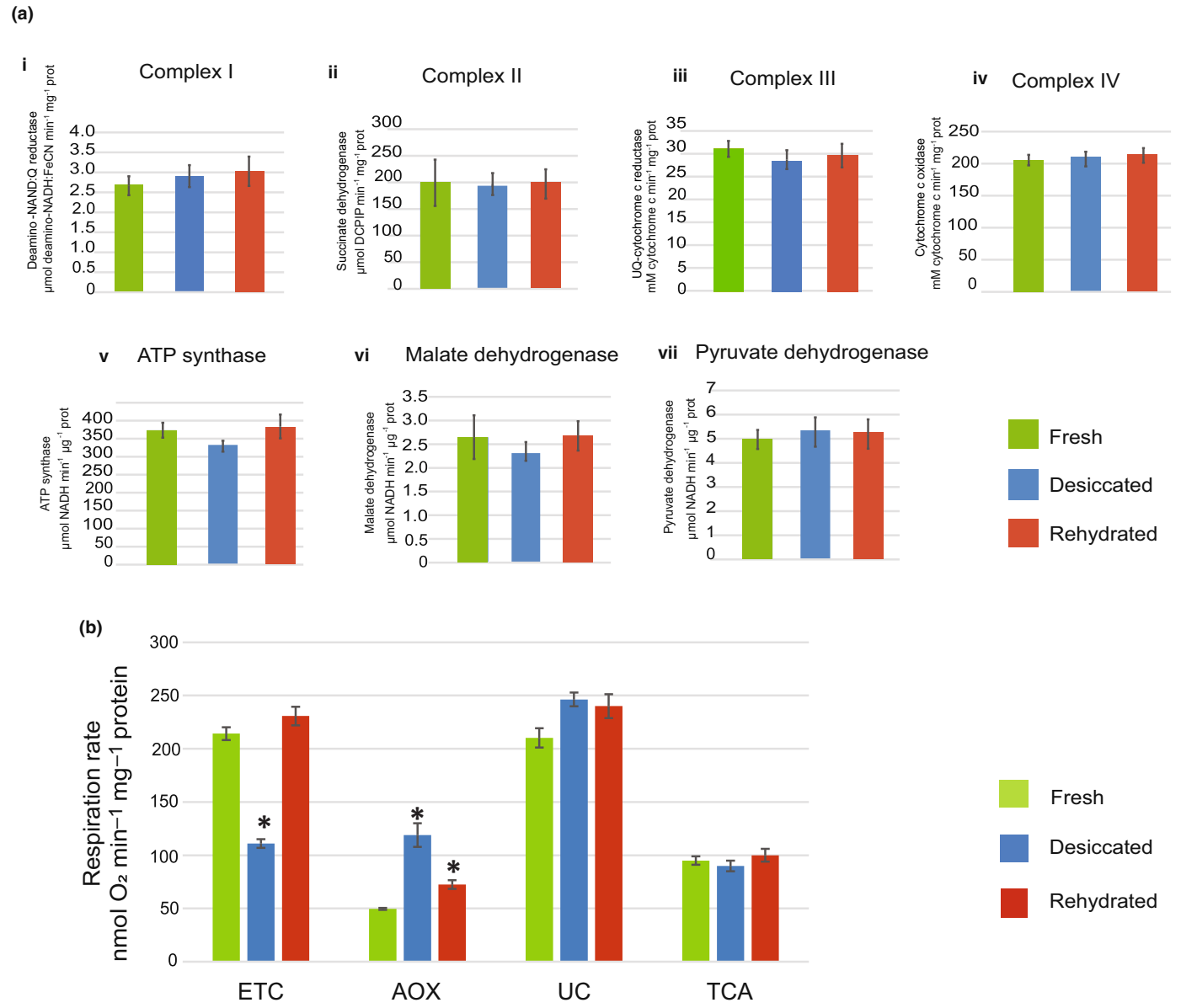

Fig. 4 Mitochondrial activities in fresh, desiccated and rehydrated *Haberlea rhodopensis* tissue. (a) Enzymatic activities of respiratory complexes and tricarboxylic acid cycle (TCA) enzymes using isolated mitochondria from fresh, desiccated and 72-h rehydrated tissues. (i) Complex I, (ii) Complex II, (iii) Complex III, (iv) Complex IV, (v) ATP synthase, (vi) malate dehydrogenase (MDC) and (vii) pyruvate dehydrogenase (PDC). Data shown are average activity per µg mg^{-1} protein (± SE, $n = 3$). (b) Oxygen consumption rates of mitochondria isolated from fresh, desiccated and 72-h rehydrated tissues. AOX, alternative oxidase; ETC, electron transport chain-linked; TCA, tricarboxylic acid cycle-linked respiration; UC, uncoupled respiration capacity. Data shown are average O_2 consumption (nmol) per min per mg protein (± SE, $n = 3$). Significant differences are indicated by *; $n = 3$, $\alpha < 0.05$, ANOVA and Tukey–Kramer's *post hoc* test.

and *TIM44* across dehydration/rehydration. (Fig. 5e). The outer membrane translocase *TOM40*, its partner protein *TOM5* and the outer membrane β-barrel translocase *METAXIN* showed constant transcript abundance (Fig. 5e). TCA cycle enzymes *MDH* and alpha subunit of pyruvate dehydrogenase (*PDC-E1*) exhibited constant levels across dehydration/rehydration (Fig. 5f) as the mitochondrial transcription RNA polymerase subunit C2, *RPO C2* and the mitochondrial fission 1, *MF1* involved in regulating mitochondrial fission (Fig. 5f).

In order to investigate the protein abundance of various components involved in mitochondrial biogenesis, immunodetection was carried out using isolated mitochondria from fresh, desiccated and 72-h post-rehydrated tissue. Analysis of the Complex I subunits, 75 kDa, CAL1, NDUFS4 and the mitochondrial-encoded NAD6 exhibited equal abundance in fresh, desiccated and rehydrated tissue (Fig. 6a). Immunodetection against Complex II subunit, SDH1-1, Complex III subunit RISP, Complex IV subunit COX2 and the β-subunit of ATP synthase likewise displayed equal protein abundance in mitochondria isolated from fresh, desiccated and rehydrated tissue (Fig. 6b). The protein import components TOM40 and the inner membrane TIM17/23 translocase subunit TIM50, showed no change in abundance

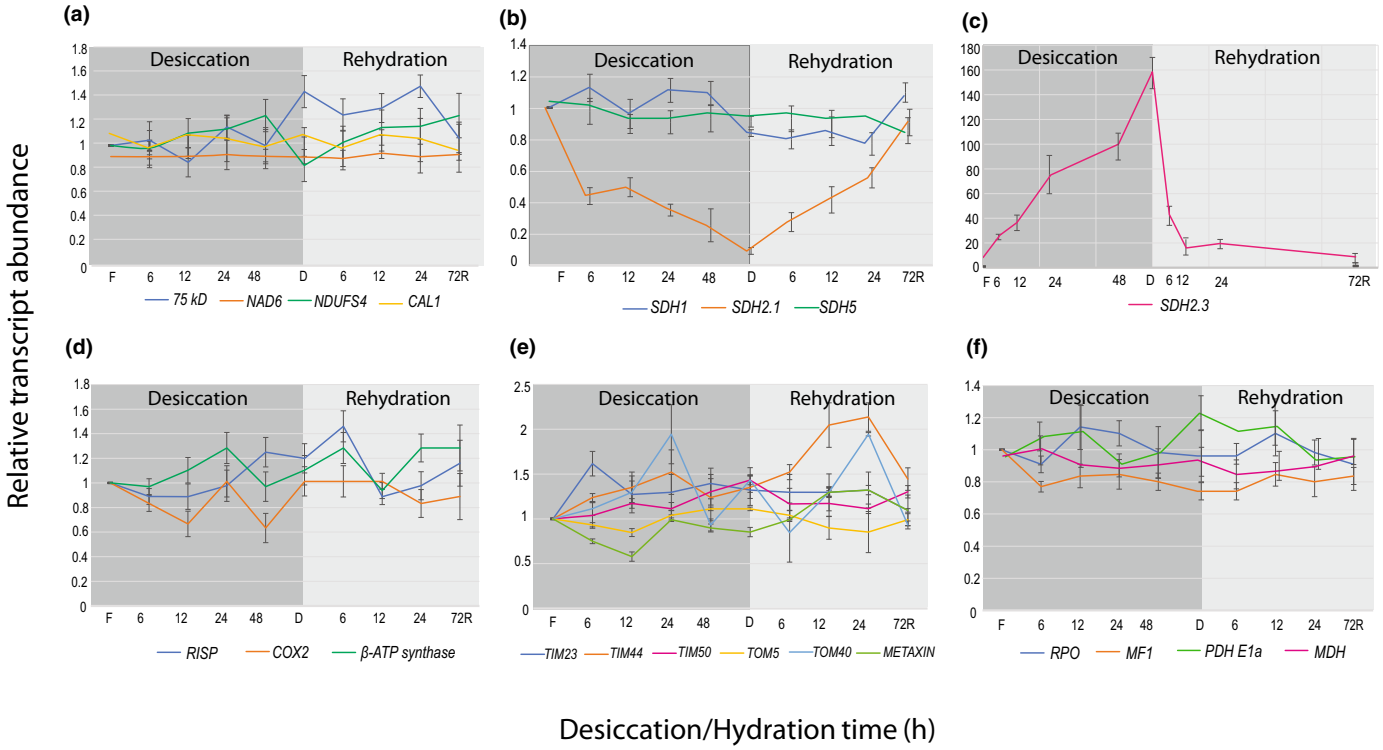

Fig. 5 Transcripts for mitochondrial components are abundant in desiccated *Haberlea rhodopensis* and remain constant during rehydration. Quantitative reverse transcription PCR (qRT-PCR) analysis of transcripts encoding (a–d) oxidative phosphorylation (OXPHOS), (e) protein import components, and (f) tricarboxylic acid cycle (TCA) cycle enzymes and mitochondrial transcription/translation factors from fresh (F), 6-,12-, 24-, 48-h dehydrated, desiccated (D) and 6-, 12-, 24- and 72-h rehydrated (R) tissue. Data shown as relative transcript abundance compared to the abundance observed in fresh tissue (± SE, $n = 3$).

across fresh, desiccated and rehydrated tissues (Fig. 6c), corresponding to the observed transcript profiles. As a control SHMT indicated equal protein loading (Fig. 6c).

Desiccation tolerance involves alternative mitochondrial respiration and stress response

Plant mitochondria also possess nonphosphorylating pathways of electron transport termed alternative oxidase (AOX) and type II NAD(P)H dehydrogenases located on different sides of the inner membrane. Alternative pathways involving AOX and/or NAD(P)H dehydrogenases operate without the translocation of protons and act as safety valves to oxidize excess reducing equivalents and prevent feedback inhibition (Vanlerberghe, 2013) which plays a significant role in alleviating stress and conferring tolerance to including drought (Giraud *et al.*, 2008; Sweetman *et al.*, 2019). To investigate if similar mechanisms play a role in desiccation tolerance, transcript and protein abundance of the mitochondrial alternative electron transport chain was investigated (Fig. 7). *Haberlea rhodopensis*, like most dicot plants, contains two AOX gene families – *AOX1* and *AOX2*. Transcript analysis of *AOX1a* and *AOX2* showed very high expression, peaking within 6 h of the dehydration and maintaining relatively high levels in desiccated tissue (Fig. 7a i) with a gradual decrease over the hydration time-course. Analysis of the internal inner membrane-located NADH dehydrogenase *NDA1* and the external intermembrane space facing *NDB2* also showed highest abundance at 12 h of dehydration, decreasing > 5-fold 72 h post-hydration (Fig. 7a ii). In addition to alternative oxidation, plant mitochondria possess plant uncoupling mitochondrial protein (UCP) that uncouples ATP production from electron transport (Ježek *et al.*, 2000; Sluse & Jarmuszkiewicz, 2002). Transcript abundance of *UCP* during dehydration and rehydration show the highest abundance of all three genes in desiccated tissue, decreasing > 2-fold 72 h post-hydration (Fig. 7a iii).

Genes known to be highly responsive during dehydration and desiccation also were analyzed (Fig. 7a iv–vi). The cytosolic late embryogenesis abundant 29 (LEA29) protein was observed to gradually increase during the dehydration process reaching a maximum in fully desiccated leaves that exceeded by 200-fold the transcript abundance in fresh tissue, decreasing rapidly after 6 h of hydration (Fig. 7a iv). The transcript abundance of the mitochondrially located superoxide dismutase (MnSOD) showed maximum abundance in desiccated leaves (Fig. 7a v). Sucrose synthase, a desiccation marker previously used for *H. rhodopensis* (Gechev *et al.*, 2021) was observed to increase during dehydration (*c.* 50-fold), decreasing to pre-desiccation levels following hydration (Fig. 7a vi). Immunodetection of AOX, NDA1, NDB2 and UCP on isolated mitochondria from fresh, desiccated and 72-h rehydrated tissue showed AOX, NDA1, NDB2 and UCP protein abundance to increase 2–4-fold in desiccated tissue, correlating to the trends observed in transcripts (Fig. 7b).

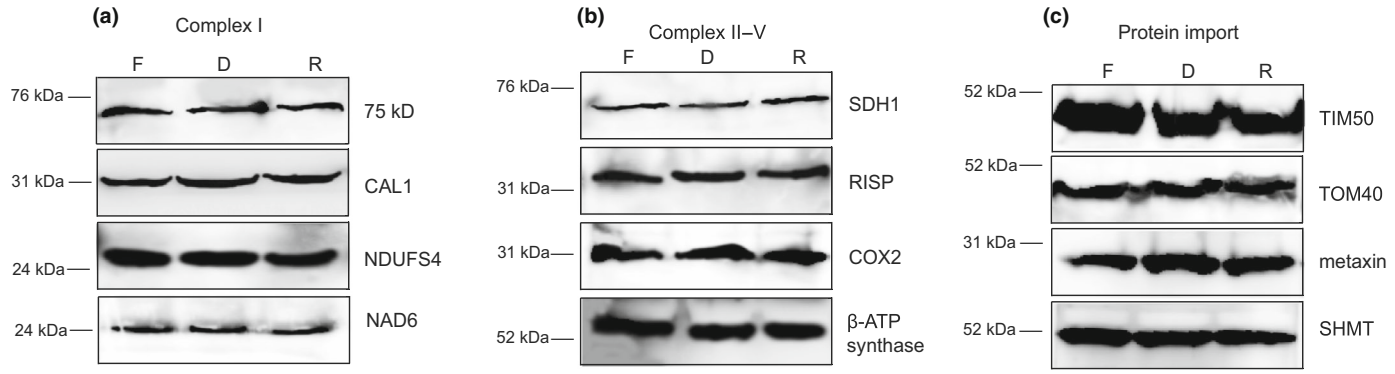

Fig. 6 Mitochondrial oxidative phosphorylation (OXPHOS) and biogenesis components are comparable in abundance in fresh, desiccated and rehydrated *Haberlea rhodopensis* mitochondria. Immunodetection of isolated mitochondria from detached fresh (F) desiccated (D) and rehydrated (R) (72-h) tissue. (a) Complex I subunits; 75 kDa, Carbonic anhydrase-like 1 (CAL1), NADH:ubiquinone oxidoreductase iron sulfur protein 4 (NDUFS4) and NADH Dehydrogenase 6 (NAD6) (b) Complex II Succinate Dehydrogenase subunit 1 (SDH1), Complex III Rieske iron sulfur protein (RISP), Complex IV Cytochrome c oxidase (COX2) and Complex V β-subunit of ATP synthase (β-ATP), (c) Protein import components translocase of the inner membrane 50 (TIM50), translocase of the outer membrane 40 (TOM40) and metaxin. Serine hydroxymethyltransferase (SHMT) was used as a loading control.

Discussion

In general, upon dehydration, plants undergo morphological and metabolic changes in response to decreased water loss, photosynthesis and respiration, in addition to the activation of protective mechanisms. During severe desiccation, sensitive plants are unable to recover whereas resurrection plants maintain cellular integrity, thus being able to recover upon rehydration. Characterization of the protective mechanisms in detached *H. rhodopensis* leaves during desiccation with a subsequent recovery during hydration identified a distinct role for mitochondria during this process. Although mitochondria in fully desiccated leaves are not active (Fig. S1b iii), upon rehydration mitochondrial respiration and activity is activated almost immediately (Figs 1b, 4, S4). By contrast, photosynthetic activity and ETR were observed to progressively increase and to reach a maximum level 60–72 h post-hydration, corresponding to 80% recovery of the IFW (Figs 1, S1a). The results from the overall physiological measurements were consistent with the observations from the organelle morphological analysis. Transmission electron micrographs revealed mitochondria containing electron-dense cristae structures (albeit smaller) in desiccated tissue, like those observed in the fresh and rehydrated tissue. Previous studies also revealed intact mitochondria with defined cristae morphology during the desiccation of *C. wilmsii*, *M. flabellifolius* and *X. humilis* (Farrant, 2000).

A detailed analysis of activity, protein and transcript abundance of genes encoding proteins involved in respiration, mitochondrial biogenesis and TCA cycle revealed that there were no significant differences between fresh, desiccated and fully hydrated tissue during both dehydration and rehydration processes. Oxygen consumption in desiccated leaves was not detected (Fig. S1b iii), but upon mitochondrial isolation, respiration rates were already at half those of fresh tissue, suggesting that the capacity for respiration including oxidative phosphorylation of ADP was present in desiccated tissue (Figs 4, S4a,b). This suggests that in *H. rhodopensis* dehydration does not cause any major degradation of mitochondrial components and cytosolic-located transcripts encoding mitochondrial proteins. Comparison of the dehydration rates between *H. rhodopensis* and its relative, nonresurrecting species *Deinostigma eberhardtii* (Kuroki *et al.*, 2019) demonstrates that in *H. rhodopensis* dehydration is much faster, with water content decreasing to 15% within 24 h. Furthermore, the molecular structure of water changes during the dehydration and rehydration process. Near-infrared spectroscopy analysis of water during desiccation revealed permanent loss of free water structures in *D. eberhardtii* whereas in *H. rhodopensis* the loss of free water was accompanied by accumulation of water molecules containing four hydrogen bonds and water dimers. This process was fully reversible upon rehydration (Kuroki *et al.*, 2019). At the same time, the accumulation of LEA proteins, with low number of intramolecular hydrogen bonds that interact with water, other proteins, or cellular components, stabilizing their structure, may act as water replacement allowing for a preservation of tissues. Desiccation tolerance of *H. rhodopensis* also has been linked to high sucrose and raffinose accumulation, shown to prevent conformational changes to proteins and membranes (Müller *et al.*, 1997; Djilianov *et al.*, 2011). Combined with the loss of free water molecules, these dynamic changes during dehydration allow for a rapid preservation of cellular integrity, which in turn results in an almost immediate reactivation of mitochondrial function at rehydration, as we have shown here.

In this study, the only difference in mitochondrial composition between fresh, desiccated and rehydrated tissues were related to the abundance of alternative respiratory pathway components and the alternative respiratory capacity. Both transcripts and protein abundance of alternative pathway components were higher in desiccated tissue. The data from the transcript and protein analyses correlate with the results from the mitochondrial functional analyses. Mitochondria isolated from desiccated tissue exhibited 2.5-fold higher AOX as well as 25% higher total uncoupled capacities in comparison with the mitochondria from fresh tissue (Figs 4, S4a). Mitochondrial alternative pathways provide the respiratory system with a flexible degree of coupling between carbon metabolism pathways, ETC activity and ATP

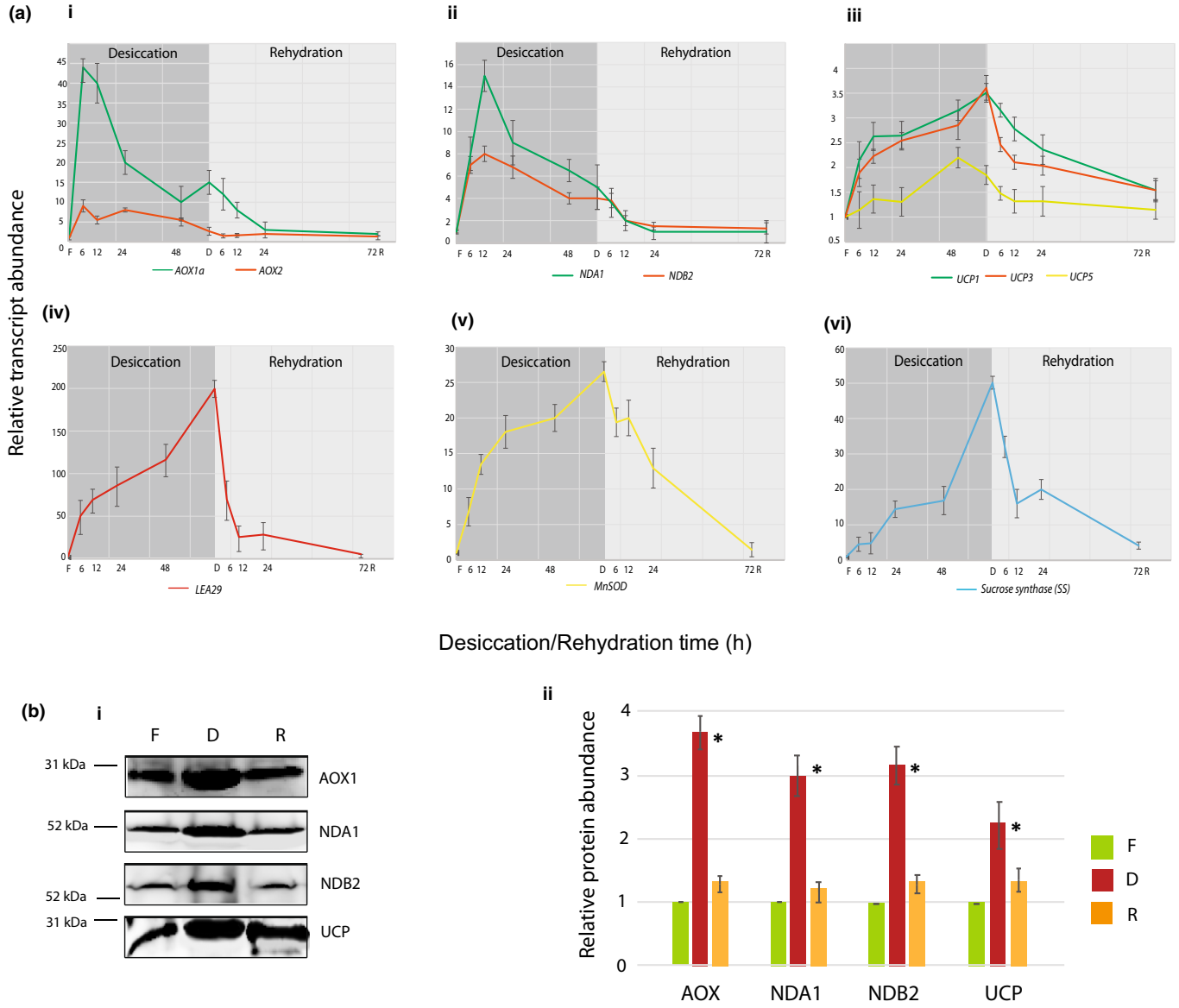

Fig. 7 Mitochondrial alternative respiratory pathways and antioxidant mechanisms are activated in desiccated *Haberlea rhodopensis* tissue. (a) Transcript abundance of various mitochondrial components in fresh (F), 6-, 12-, 24-, 48-h dehydrated, desiccated (D) and 6-, 12-, 24- and 72-h rehydrated (R) detached leaf tissue. Quantitative reverse transcription (qRT)-PCR analysis of transcripts encoding the (i) Alternative Oxidase (*AOX1a* and *AOX2*), (ii) type II NAD(P)H dehydrogenases (*NDA1* and *NDB2*), (iii) uncoupling proteins (*UCP1, UCP2* and *UCP5*), (iv) late embryogenesis abundant protein (*LEA29*), (v) superoxide dismutase (*MnSOD*) and (vi) sucrose synthase (*SS*). Data shown as relative transcript abundance compared to the abundance observed in fresh tissue ± SE, $n = 3$. (b) (i) Immunodetection of isolated mitochondria from fresh (F), desiccated (D) and 72-h rehydrated (R) detached leaves with antibodies raised against Arabidopsis alternative respiratory subunits AOX, NDA1, NDB2, mitochondrial uncoupling protein UCP. (ii) Relative protein abundance from desiccated and rehydrated tissue compared to fresh tissue is shown. Significant differences indicated by *: $n = 3$; mean ± SE, $\alpha < 0.05$, ANOVA and Tukey–Kramer's *post hoc* test.

turnover. A variety of studies have concluded that alternative respiratory pathways function in metabolic and signalling homeostasis, which are particularly important during adverse growth conditions. Alternative oxidase lowers mitochondrial ROS production by preventing over-reduction of the electron transport chain components (Selinski *et al.*, 2018). At the same time AOX activity can regulate mitochondrial signalling molecules such as superoxide and nitric oxide, providing mitochondria with a means of retrograde signalling to influence nuclear gene expression and initiate acclimation strategies (Vanlerberghe, 2013). It is well-documented that AOX1 is highly responsive to abiotic and biotic stresses, as well as respiratory metabolism dysfunction (Clifton *et al.*, 2006), whereas AOX2 generally is not stress-responsive and instead, is expressed in reproductive tissues and seeds (Saish *et al.*, 2001; Chai *et al.*, 2010). Unexpectedly, we found that both *AOX1* and *AOX2* exhibited the highest expression levels soon after the onset of desiccation keeping relatively high levels in desiccated vegetative tissue that gradually decreased during rehydration, suggesting a role for both AOXs in desiccation tolerance. This is supported by transcriptomic profiling of

C. plantagineum that likewise showed *AOX2* abundance increasing > 3-fold in desiccated tissue compared to rehydrated tissue (Xu *et al.*, 2021).

In addition to AOX, plant mitochondria contain several type II NAD(P)H dehydrogenases which also are involved in uncoupling electron transfer from ATP synthesis. Together with AOX, type II NAD(P)H dehydrogenases are upregulated following mitochondrial stress to help minimize ROS production and prevent feedback inhibition of metabolism (Clifton *et al.*, 2006; Vanlerberghe, 2013). Likewise, we observed maximum transcript abundance of NAD(P)H dehydrogenases shortly after water depravation which decreased during rehydration (Fig. 7). Overexpression of *NDB2* alongside *AOX* increased Arabidopsis tolerance to drought stress (Sweetman *et al.*, 2019) supporting the role of mitochondrial NAD(P)H dehydrogenases in being induced upon water limitation. In Arabidopsis the negative impact of severe salinity stress on photosynthetic capacity did not differ between wild-type and a double mutant *aox1a::aox1d* while the stress was ongoing, but only during recovery with plants with inhibited AOX1 activity not being able to recover (Oh *et al.*, 2022).

Mitochondrial UCP proteins are inner membrane-located carrier proteins that pump protons across the inner membrane to uncouple electron transport from ATP synthesis. Uncoupling mitochondrial protein proteins have been shown to play a role during plant stress, suppressing mitochondrial ROS formation (Barreto *et al.*, 2020). Interestingly, drought tolerance (and reduced ROS concentrations) could be achieved by the overexpression of Arabidopsis UCP1 in tobacco (Begcy *et al.*, 2011). It was found that mitochondrial UCP displayed its highest transcript and protein abundance in desiccated tissue, suggesting that these proteins also may play a role in maintaining desiccation tolerance. Evidently *H. rhodopensis* activates numerous mitochondrial protective and stress responsive mechanisms to protect mitochondria from oxidative damage and to preserve respiration mechanisms under desiccation.

Acquisition of vegetative desiccation tolerance via seed desiccation mechanisms

Studies of resurrecting plants reveal that the mechanisms and pathways required for vegetative desiccation tolerance, overlap with mechanisms utilized by seeds (Costa *et al.*, 2017; Lyall & Gechev, 2020). It is proposed that seed desiccation tolerance originated from ancestral vegetative desiccation tolerance found in early land plants (Oliver *et al.*, 2005), and that angiosperm resurrection plants acquired their tolerance by re-activating innate seed desiccation tolerance mechanisms in their vegetative tissues (Farrant & Moore, 2011; Costa *et al.*, 2017). With respect to desiccation tolerance, transcriptome studies in *Solanum lycopersicum*, *Medicago truncatula* and Arabidopsis reveal genes encoding mitochondrial proteins such as LEA and HSP, as well as ABA-responsive and antioxidant components associated with desiccation tolerance (Barbagallo *et al.*, 2003; Terrasson *et al.*, 2013; Gonzalez-Morales *et al.*, 2016). This is consistent with similar mechanisms and pathways thought to confer desiccation tolerance in seeds and resurrection plants (Stupnikova *et al.*, 2006; Macherel *et al.*, 2007; Georgieva *et al.*, 2017; Kijak & Ratajczak, 2020; Stavrinides *et al.*, 2020).

Mitochondria play an essential role during seed development, maturation and germination, yet there are significant differences in desiccation tolerance between tissue and seed mitochondria. During seed desiccation, mitochondria undergo a co-ordinated shut down of metabolic functions (Stavrinides *et al.*, 2020). In dry seeds, mitochondria often termed promitochondria are present, but poorly differentiated and contain few cristae structures (Logan *et al.*, 2001; Howell *et al.*, 2006; W. G. Wang *et al.*, 2012). Although bioenergetic reactivation of promitochondria, determined by presence of a membrane potential, is immediate upon rehydration (Paszkiewicz *et al.*, 2017), mitochondrial biogenesis is activated progressively, displaying a steady increase of transcripts and proteins involved in transcription, translation, protein import and respiration upon imbibition (Narsai *et al.*, 2011; Law *et al.*, 2012, 2014). By contrast, we found that mitochondrial ultrastructure in desiccated *H. rhodopensis* was well-preserved with intact cristae structures. Upon re-hydration, mitochondrial respiration and activity were activated immediately reaching maximum levels within 30 min, comparable to those observed in fresh leaves. Furthermore, the abundance of various mitochondrial respiratory chain and protein import components were present at high levels in desiccated tissue and OXPHOS complexes were fully assembled, suggesting that during *H. rhodopensis* desiccation mitochondrial function is not accompanied by a decrease in capacity that needs to be re-established on re-hydration.

Interestingly, the two homologues of SDH2 displayed opposing expression profiles during desiccation and rehydration compared to all other OXPHOS subunits tested. SDH2.1 exhibited a decrease during dehydration, followed by steady increase during the rehydration whilst SDH2.3 abundance increased during desiccation followed by a sharp decrease (> 120-fold) within 6 h of rehydration. This suggests that the preferred homologue during desiccation is SDH2.3 which may play a protective role during desiccation. Likewise, in Arabidopsis, SDH2 is encoded by three homologues, *SDH2.1* and *SDH2.2*, primarily expressed in vegetative tissues, and *SDH2.3* only expressed in seeds (Elorza *et al.*, 2004, 2006). It has been shown that SDH2.3 is the most abundant protein in dry seed mitochondria declining during germination to be subsequently replaced by SDH2-1/2 (Restovic *et al.*, 2017; Heidorn-Czarna *et al.*, 2018). This suggests that SDH2.3 may play a unique role in seed desiccation tolerance, perhaps by providing Complex II with increased structural stability during the dry state (Macherel *et al.*, 2007) a mechanism probably re-purposed in *H. rhodopensis*.

Here, we investigated the role of mitochondria during desiccation and rehydration of *H. rhodopensis* detached leaves. We found that the mitochondrial ultrastructure, activity, transcript and protein abundances were preserved in desiccated tissue and maintained during rehydration. This supports the conclusion that mitochondria from *H. rhodopensis* vegetative leaves are conserved in a functional state during desiccation, allowing for rapid activation upon rehydration. We identified mitochondria-specific mechanisms such as the induction of high alternative respiratory

pathways, probably a protective mechanism correlating with rapid recovery following rehydration.

Acknowledgements

AI is supported by the Peter Beron I NIE Programme, Bulgarian National Science Fund (KP-06-DB-6/2019). MWM is supported by a Research Council Discovery Grants (DP200101922 and DP210103258). JW is supported by an Australian Research Council Discovery Grant (DP200102452). SS is an active member of the Uruguayan System of Researchers (SNI, Uruguay). Open access publishing facilitated by The University of Western Australia, as part of the Wiley - The University of Western Australia agreement via the Council of Australian University Librarians.

Author contributions

AI, DD and MWM planned and designed the research; AI, BO, SS and DF performed experiments; AI, DM, JW, DD and MWM analyzed the data and all authors contributed to the preparation of the manuscript.

ORCID

Dimitar Djilianov https://orcid.org/0000-0001-6492-8033
Denis Falconet https://orcid.org/0000-0001-8182-1182
Aneta Ivanova https://orcid.org/0000-0002-2465-7213
Daniela Moyankova https://orcid.org/0000-0003-4020-1918
Monika W. Murcha https://orcid.org/0000-0002-3689-6158
Brendan O'Leary https://orcid.org/0000-0002-8770-155X
Santiago Signorelli https://orcid.org/0000-0002-1854-3164
James Whelan https://orcid.org/0000-0001-5754-025X

Data availability

The data that support the findings of this study are available in the Supporting information of this article. The author responsible for distribution of materials integral to the findings presented in this article is MWM.

References

Barbagallo RP, Oxborough K, Pallett KE, Baker NR. 2003. Rapid, noninvasive screening for perturbations of metabolism and plant growth using chlorophyll fluorescence imaging. *Plant Physiology* **132**: 485–493.

Barreto P, Couñago RM, Arruda P. 2020. Mitochondrial uncoupling protein-dependent signaling in plant bioenergetics and stress response. *Mitochondrion* **53**: 109–120.

Begcy K, Mariano ED, Mattiello L, Nunes AV, Mazzafera P, Maia IG, Menossi M. 2011. An Arabidopsis mitochondrial uncoupling protein confers tolerance to drought and salt stress in transgenic tobacco plants. *PLoS ONE* **6**: e23776.

Carrie C, Giraud E, Duncan O, Xu L, Wang Y, Huang S, Clifton R, Murcha M, Filipovska A, Rackham O *et al.* 2010. Conserved and novel functions for *Arabidopsis thaliana* MIA40 in assembly of proteins in mitochondria and peroxisomes. *The Journal of Biological Chemistry* **285**: 36138–36148.

Carrie C, Kuhn K, Murcha MW, Duncan O, Small ID, O'Toole N, Whelan J. 2009. Approaches to defining dual-targeted proteins in Arabidopsis. *The Plant Journal* **57**: 1128–1139.

Carrie C, Murcha MW, Kuehn K, Duncan O, Barthet M, Smith PM, Eubel H, Meyer E, Day DA, Millar AH *et al.* 2008. Type II NAD(P)H dehydrogenases are targeted to mitochondria and chloroplasts or peroxisomes in *Arabidopsis thaliana*. *FEBS Letters* **582**: 3073–3079.

Catterall WA, Coty WA, Pedersen PL. 1973. Adenosine triphosphatase from rat liver mitochondria. 3. Subunit composition. *Journal of Biological Chemistry* **248**: 7427–7431.

Catterall WA, Pedersen PL. 1971. Adenosine triphosphatase from rat liver mitochondria. I. Purification, homogeneity, and physical properties. *The Journal of Biological Chemistry* **246**: 4987–4994.

Chai TT, Simmonds D, Day DA, Colmer TD, Finnegan PM. 2010. Photosynthetic performance and fertility are repressed in GmAOX2b antisense soybean. *Plant Physiology* **152**: 1638–1649.

Challabathula D, Zhang Q, Bartels D. 2018. Protection of photosynthesis in desiccation-tolerant resurrection plants. *Journal of Plant Physiology* **227**: 84–92.

Clifton R, Millar AH, Whelan J. 2006. Alternative oxidases in Arabidopsis: a comparative analysis of differential expression in the gene family provides new insights into function of non-phosphorylating bypasses. *Biochimica et Biophysica Acta* **1757**: 730–741.

Considine MJ, Daley DO, Whelan J. 2001. The expression of alternative oxidase and uncoupling protein during fruit ripening in mango. *Plant Physiology* **126**: 1619–1629.

Costa MD, Cooper K, Hilhorst HWM, Farrant JM. 2017. Orthodox seeds and resurrection plants: two of a kind? *Plant Physiology* **175**: 589–599.

Dinakar C, Djilianov D, Bartels D. 2012. Photosynthesis in desiccation tolerant plants: energy metabolism and antioxidative stress defense. *Plant Science* **182**: 29–41.

Djilianov D, Genova G, Parvanova D, Zapryanova N, Konstantinova T, Atanassov A. 2005. *In vitro* culture of the resurrection plant *Haberlea rhodopensis*. *Plant Cell, Tissue and Organ Culture* **80**: 115–118.

Djilianov D, Ivanov S, Moyankova D, Miteva L, Kirova E, Alexieva V, Joudi M, Peshev D, Van den Ende W. 2011. Sugar ratios, glutathione redox status and phenols in the resurrection species *Haberlea rhodopensis* and the closely related non-resurrection species *Chirita eberhardtii*. *Plant Biology* **13**: 767–776.

Elorza A, Leon G, Gomez I, Mouras A, Holuigue L, Araya A, Jordana X. 2004. Nuclear SDH2-1 and SDH2-2 genes, encoding the iron-sulfur subunit of mitochondrial complex II in Arabidopsis, have distinct cell-specific expression patterns and promoter activities. *Plant Physiology* **136**: 4072–4087.

Elorza A, Roschzttardtz H, Gomez I, Mouras A, Holuigue L, Araya A, Jordana X. 2006. A nuclear gene for the iron-sulfur subunit of mitochondrial complex II is specifically expressed during Arabidopsis seed development and germination. *Plant & Cell Physiology* **47**: 14–21.

Elthon TE, Nickels RL, McIntosh L. 1989. Monoclonal antibodies to the alternative oxidase of higher plant mitochondria. *Plant Physiology* **89**: 1311–1317.

Eubel H, Braun HP, Millar AH. 2005. Blue-native PAGE in plants: a tool in analysis of protein-protein interactions. *Plant Methods* **1**: 11.

Farrant JM. 2000. A comparison of mechanisms of desiccation tolerance among three angiosperm resurrection plant species. *Plant Ecology* **151**: 29–39.

Farrant JM, Moore JP. 2011. Programming desiccation-tolerance: from plants to seeds to resurrection plants. *Current Opinion in Plant Biology* **14**: 340–345.

Flori S, Jouneau PH, Gallet B, Estrozi LF, Moriscot C, Schoehn G, Finazzi G, Falconet D. 2018. Imaging plastids in 2D and 3D: confocal and electron microscopy. *Methods in Molecular Biology* **1829**: 113–122.

Forlani G, Trovato M, Funck D, Signorelli S. 2019. Regulation of proline accumulation and its molecular and physiological functions in stress defence. In: Hossain MA, Kumar V, Burritt DJ, Fujita M, Mäkelä PSA, eds. *Osmoprotectant-mediated abiotic stress tolerance in plants: recent advances and future perspectives*. Cham, Switzerland: Springer International, 73–97.

Gaff DF, Oliver M. 2013. The evolution of desiccation tolerance in angiosperm plants: a rare yet common phenomenon. *Functional Plant Biology* **40**: 315–328.

Gechev T, Lyall R, Petrov V, Bartels D. 2021. Systems biology of resurrection plants. *Cellular and Molecular Life Sciences* **78**: 6365–6394.

Gechev TS, Benina M, Obata T, Tohge T, Sujeeth N, Minkov I, Hille J, Temanni MR, Marriott AS, Bergstrom E *et al.* 2013. Molecular mechanisms

of desiccation tolerance in the resurrection glacial relic *Haberlea rhodopensis*. *Cellular and Molecular Life Sciences* **70**: 689–709.

Georgieva K, Dagnon S, Gesheva E, Bojilov D, Mihailova G, Doncheva S. 2017. Antioxidant defense during desiccation of the resurrection plant *Haberlea rhodopensis*. *Plant Physiology and Biochemistry* **114**: 51–59.

Georgieva K, Mihailova G, Velitchkova M, Popova A. 2020. Recovery of photosynthetic activity of resurrection plant *Haberlea rhodopensis* from drought- and freezing-induced desiccation. *Photosynthetica* **58**: 911–921.

Giraud E, Ho LH, Clifton R, Carroll A, Estavillo G, Tan YF, Howell KA, Ivanova A, Pogson BJ, Millar AH *et al.* 2008. The absence of ALTERNATIVE OXIDASE1a in Arabidopsis results in acute sensitivity to combined light and drought stress. *Plant Physiology* **147**: 595–610.

Gonzalez-Morales SI, Chavez-Montes RA, Hayano-Kanashiro C, Alejo-Jacuinde G, Rico-Cambron TY, de Folter S, Herrera-Estrella L. 2016. Regulatory network analysis reveals novel regulators of seed desiccation tolerance in *Arabidopsis thaliana*. *Proceedings of the National Academy of Sciences, USA* **113**: E5232–E5241.

Heidorn-Czarna M, Domanski D, Kwasniak-Owczarek M, Janska H. 2018. Targeted proteomics approach toward understanding the role of the mitochondrial protease FTSH4 in the biogenesis of OXPHOS during Arabidopsis seed germination. *Frontiers in Plant Science* **9**: 821.

Höfler K, MH, Rottenburg W. 1941. Über die Austrocknungresistenz landwirtschaftlicher Kulturpflanzen. *Forschung* **12**: 50–61.

Howell KA, Millar AH, Whelan J. 2006. Ordered assembly of mitochondria during rice germination begins with pro-mitochondrial structures rich in components of the protein import apparatus. *Plant Molecular Biology* **60**: 201–223.

Huang S, Lee CP, Millar AH. 2015. Activity assay for plant mitochondrial enzymes. *Methods in Molecular Biology* **1305**: 139–149.

Jacoby RP, Millar AH, Taylor NL. 2015. Assessment of respiration in isolated plant mitochondria using Clark-type electrodes. *Methods in Molecular Biology* **1305**: 165–185.

Ježek P, Žáčková M, Košařová J, Rodrigues ETS, Madeira VMC, Vicente JAF. 2000. Occurrence of plant-uncoupling mitochondrial protein (PUMP) in diverse organs and tissues of several plants. *Journal of Bioenergetics and Biomembranes* **32**: 549–561.

Kijak H, Ratajczak E. 2020. What do we know about the genetic basis of seed desiccation tolerance and longevity? *International Journal of Molecular Sciences* **21**: 3612.

Koonjul P, Brandt W, Farrant J. 2000. Isolation and characterisation of chloroplasts from *Myrothamnus flabellifolius* Welw. *Journal of Plant Physiology* **156**: 584–594.

Kuroki S, Tsenkova R, Moyankova D, Muncan J, Morita H, Atanassova S, Djilianov D. 2019. Water molecular structure underpins extreme desiccation tolerance of the resurrection plant *Haberlea rhodopensis*. *Scientific Reports* **9**: 3049.

Lamattina L, Gonzalez D, Gualberto J, Grienenberger JM. 1993. Higher plant mitochondria encode an homologue of the nuclear-encoded 30-kDa subunit of bovine mitochondrial complex I. *European Journal of Biochemistry* **217**: 831–838.

Law SR, Narsai R, Taylor NL, Delannoy E, Carrie C, Giraud E, Millar AH, Small I, Whelan J. 2012. Nucleotide and RNA metabolism prime translational initiation in the earliest events of mitochondrial biogenesis during Arabidopsis germination. *Plant Physiology* **158**: 1610–1627.

Law SR, Narsai R, Whelan J. 2014. Mitochondrial biogenesis in plants during seed germination. *Mitochondrion* **19**: 214–221.

Lister R, Carrie C, Duncan O, Ho LH, Howell KA, Murcha MW, Whelan J. 2007. Functional definition of outer membrane proteins involved in preprotein import into mitochondria. *Plant Cell* **19**: 3739–3759.

Liu J, Moyankova D, Lin CT, Mladenov P, Sun RZ, Djilianov D, Deng X. 2018. Transcriptome reprogramming during severe dehydration contributes to physiological and metabolic changes in the resurrection plant *Haberlea rhodopensis*. *BMC Plant Biology* **18**: 351.

Logan DC, Millar AH, Sweetlove LJ, Hill SA, Leaver CJ. 2001. Mitochondrial biogenesis during germination in maize embryos. *Plant Physiology* **125**: 662–672.

Luo C, Long J, Liu J. 2008. An improved spectrophotometric method for a more specific and accurate assay of mitochondrial complex III activity. *Clinica Chimica Acta* **395**: 38–41.

Lyall R, Gechev T. 2020. Multi-omics insights into the evolution of angiosperm resurrection plants. In: Roberts JA, ed. *Annual plant reviews online, vol. 3*. New York, NY, USA: Wiley. doi: 10.1002/9781119312994.apr0730.

Macherel D, Benamar A, Avelange-Macherel M-H, Tolleter D. 2007. Function and stress tolerance of seed mitochondria. *Physiologia Plantarum* **129**: 233–241.

Martinelli T. 2008. *In situ* localization of glucose and sucrose in dehydrating leaves of *Sporobolus stapfianus*. *Journal of Plant Physiology* **165**: 580–587.

Mladenov P, Finazzi G, Bligny R, Moyankova D, Zasheva D, Boisson AM, Brugiere S, Krasteva V, Alipieva K, Simova S *et al.* 2015. *In vivo* spectroscopy and NMR metabolite fingerprinting approaches to connect the dynamics of photosynthetic and metabolic phenotypes in resurrection plant *Haberlea rhodopensis* during desiccation and recovery. *Frontiers in Plant Science* **6**: 564.

Moyankova D, Mladenov P, Berkov S, Peshev D, Georgieva D, Djilianov D. 2014. Metabolic profiling of the resurrection plant *Haberlea rhodopensis* during desiccation and recovery. *Physiologia Plantarum* **152**: 675–687.

Müller J, Sprenger N, Bortlik K, Boller T, Wiemken A. 1997. Desiccation increases sucrose levels in Ramonda and Haberlea, two genera of resurrection plants in the Gesneriaceae. *Physiologia Plantarum* **100**: 153–158.

Nadal M, Perera-Castro AV, Gulias J, Farrant JM, Flexas J. 2021. Resurrection plants optimize photosynthesis despite very thick cell walls by means of chloroplast distribution. *Journal of Experimental Botany* **72**: 2600–2610.

Narsai R, Law SR, Carrie C, Xu L, Whelan J. 2011. In-depth temporal transcriptome profiling reveals a crucial developmental switch with roles for RNA processing and organelle metabolism that are essential for germination in Arabidopsis. *Plant Physiology* **157**: 1342–1362.

Oh GGK, O'Leary BM, Signorelli S, Millar AH. 2022. Alternative oxidase (AOX) 1a and 1d limit proline-induced oxidative stress and aid salinity recovery in Arabidopsis. *Plant Physiology* **188**: 1521–1536.

O'Leary BM, Lee CP, Atkin OK, Cheng R, Brown TB, Millar AH. 2017. Variation in leaf respiration rates at night correlates with carbohydrate and amino acid supply. *Plant Physiology* **174**: 2261–2273.

Oliver MJ, Farrant JM, Hilhorst HWM, Mundree S, Williams B, Bewley JD. 2020. Desiccation tolerance: avoiding cellular damage during drying and rehydration. *Annual Review of Plant Biology* **71**: 435–460.

Oliver MJ, Velten J, Mishler BD. 2005. Desiccation tolerance in bryophytes: a reflection of the primitive strategy for plant survival in dehydrating habitats? *Integrative and Comparative Biology* **45**: 788–799.

Paszkiewicz G, Gualberto JM, Benamar A, Macherel D, Logan DC. 2017. Arabidopsis seed mitochondria are bioenergetically active immediately upon imbibition and specialize via biogenesis in preparation for autotrophic growth. *Plant Cell* **29**: 109–128.

Restovic F, Espinoza-Corral R, Gomez I, Vicente-Carbajosa J, Jordana X. 2017. An active mitochondrial complex II present in mature seeds contains an embryo-specific iron-sulfur subunit regulated by ABA and bZIP53 and is involved in germination and seedling establishment. *Frontiers in Plant Science* **8**: 277.

Saish D, Nakazono M, Lee KH, Tsutsumi N, Akita S, Hirai A. 2001. The gene for alternative oxidase-2 (AOX2) from *Arabidopsis thaliana* consists of five exons unlike other AOX genes and is transcribed at an early stage during germination. *Genes & Genetic Systems* **76**: 89–97.

Scafaro AP, Negrini ACA, O'Leary B, Rashid FAA, Hayes L, Fan Y, Zhang Y, Chochois V, Badger MR, Millar AH *et al.* 2017. The combination of gas-phase fluorophore technology and automation to enable high-throughput analysis of plant respiration. *Plant Methods* **13**: 16.

Selinski J, Scheibe R, Day DA, Whelan J. 2018. Alternative oxidase is positive for plant performance. *Trends in Plant Science* **23**: 588–597.

Senkler J, Senkler M, Eubel H, Hildebrandt T, Lengwenus C, Schertl P, Schwarzlander M, Wagner S, Wittig I, Braun HP. 2017. The mitochondrial complexome of *Arabidopsis thaliana*. *The Plant Journal* **89**: 1079–1092.

Sluse FE, Jarmuszkiewicz W. 2002. Uncoupling proteins outside the animal and plant kingdoms: functional and evolutionary aspects. *FEBS Letters* **510**: 117–120.

Soole KL, Smith CA. 2015. Analysis of type II NAD(P)H dehydrogenases. *Methods in Molecular Biology* **1305**: 151–164.

Stavrinides AK, Dussert S, Combes MC, Fock-Bastide I, Severac D, Minier J, Bastos-Siqueira A, Demolombe V, Hem S, Lashermes P *et al.* 2020. Seed

comparative genomics in three coffee species identify desiccation tolerance mechanisms in intermediate seeds. *Journal of Experimental Botany* **71**: 1418–1433.

Stupnikova I, Benamar A, Tolleter D, Grelet J, Borovskii G, Dorne AJ, Macherel D. 2006. Pea seed mitochondria are endowed with a remarkable tolerance to extreme physiological temperatures. *Plant Physiology* **140**: 326–335.

Sweetman C, Waterman CD, Rainbird BM, Smith PMC, Jenkins CD, Day DA, Soole KL. 2019. AtNDB2 is the main external NADH dehydrogenase in mitochondria and is important for tolerance to environmental stress. *Plant Physiology* **181**: 774–788.

Terrasson E, Buitink J, Righetti K, Ly Vu B, Pelletier S, Zinsmeister J, Lalanne D, Leprince O. 2013. An emerging picture of the seed desiccome: confirmed regulators and newcomers identified using transcriptome comparison. *Frontiers in Plant Science* **4**: 497.

Tuba Z, Protor M, Csintalan Z. 1998. Ecophysiological responses of homoiochlorophyllous and poikilochlorophyllous desiccation tolerant plants: a comparison and an ecological perspective. *Plant Growth Regulation* **24**: 211–217.

Tuba ZD, Smirnoff N, Csintalan Z, Szente KIN, Nagy ZK. 1997. Respiration during slow desiccation of the poikilochlorophyllous desiccation tolerant plant *Xerophyta scabrida* at present-day CO_2 concentration. *Plant Physiology and Biochemistry* **35**: 381–386.

Vanlerberghe GC. 2013. Alternative oxidase: a mitochondrial respiratory pathway to maintain metabolic and signaling homeostasis during abiotic and biotic stress in plants. *International Journal of Molecular Sciences* **14**: 6805–6847.

Wang W, Vignani R, Scali M, Cresti M. 2006. A universal and rapid protocol for protein extraction from recalcitrant plant tissues for proteomic analysis. *Electrophoresis* **27**: 2782–2786.

Wang WQ, Cheng HY, Moller IM, Song SQ. 2012. The role of recovery of mitochondrial structure and function in desiccation tolerance of pea seeds. *Physiologia Plantarum* **144**: 20–34.

Wang Y, Carrie C, Giraud E, Elhafez D, Narsai R, Duncan O, Whelan J, Murcha MW. 2012. Dual location of the mitochondrial preprotein transporters B14.7 and Tim23-2 in complex I and the TIM17:23 complex in Arabidopsis links mitochondrial activity and biogenesis. *Plant Cell* **24**: 2675–2695.

Xu X, Legay S, Sergeant K, Zorzan S, Leclercq CC, Charton S, Giarola V, Liu X, Challabathula D, Renaut J *et al.* 2021. Molecular insights into plant desiccation tolerance: transcriptomics, proteomics and targeted metabolite profiling in *Craterostigma plantagineum*. *The Plant Journal* **107**: 377–398.

Zhu Y, Berkowitz O, Selinski J, Hartmann A, Narsai R, Wang Y, Mao P, Whelan J. 2020. Conserved and opposite transcriptome patterns during germination in *Hordeum vulgare* and *Arabidopsis thaliana*. *International Journal of Molecular Sciences* **21**: 7404.

Supporting Information

Additional Supporting Information may be found online in the Supporting Information section at the end of the article.

Fig. S1 Weight loss and recovery of detached *Haberlea rhodopensis* leaves and O_2 consumption rates using 72-h rehydrated and dessicated leaves.

Fig. S2 Pearson correlation analysis between F_V/F_M and recovery and chloroplast electron transport rates for fresh, desiccated and rehydrated leaves.

Fig. S3 SDS-PAGE analysis and Coomassie staining of mitochondria isolated from *Haberlea rhodopensis* detached leaves.

Fig. S4 Examples of oxygen consumption measurements of isolated mitochondria using Clark-type electrodes.

Table S1 Quantitative reverse transcription PCR (qRT-PCR) primers used in this study.

Please note: Wiley Blackwell are not responsible for the content or functionality of any Supporting Information supplied by the authors. Any queries (other than missing material) should be directed to the *New Phytologist* Central Office.